DESALTING HIGH SALINITY SHALE FLOWBACK WATER VIA HIGH-FLUX NANOFLUIDIC EVAPORATION-CONDENSATION

Kaushik K. Rangharajan, Varun Lochab, and Shaurya Prakash*
Department of Mechanical and Aerospace Engineering, The Ohio State University, Columbus, OH, USA

ABSTRACT

A proof-of-concept nanofluidic device for desalting high salinity waters arising from shale oil/gas extraction was demonstrated. The nanofluidic device uses forward osmosis (FO) to drive an isothermal evaporation-condensation process over tunable sections of functionalized hydrophobicity inside a nanochannel. Desalting high salinity waters was demonstrated for various electrolytes but most prominently, we show direct desalting of Utica shale flowback water (equivalent salt at 3 M or > 180,000 ppm salinity). The tunable hydrophobic regions (l_h) generate vapor-traps inside nanochannels as liquid water cannot cross over the hydrophobic region. An average water flux of 47.3 $Lm^{-2}h^{-1}$ was measured compared to 10 $Lm^{-2}h^{-1}$ for state-of-art FO membranes [1] at an osmotic pressure of 48 bar with > 99% salt rejection.

INTRODUCTION

Due to rapid increase in energy demands and the need for self-sustaining domestic alternatives to gain energy independence, unconventional oil and gas industry has grown exponentially in the United States [2], with currently more than 400 operational wells in Ohio. In 2015, natural gas contributed 33% towards overall US energy demand (and was at par with coal) [3]. Natural gas power plants are commercially and environmentally more attractive as they can maintain an operational efficiency up to 58% compared to 38% for coal powered plants, in addition to reducing CO_2 emissions by half [4].

Hydraulic fracturing (HF) for shale production requires about 3-5 million gallons of water per well, where the water is mixed with various chemical agents (driller and geology dependent) and pressurized to an average depth of 6000 feet (1800 m) (Utica) [5] to instigate and keep open the thin fissures or cracks in the fractured rock-bed for resource extraction. However, 20-40% of this injected water flows back with excessive salinity (3-7x sea water) containing several toxic and radioactive species [6]. Current estimates across U.S. lead to nearly 2 billion gallons of class II (limited to oil and gas) fluids [7], that is generated daily and typically disposed *via* deep injection wells of sub-surface depth ranging from 800 – 13,000 feet, which is known to potentially trigger damaging seismic events [8].

Nearly all commercially viable salt water treatment systems are membrane based and are optimized for operation with seawater (~ 35,000 ppm salinity). High salinity or hyper-saline waters (> 80,000 ppm) arising from shale plays (Table 1) pose extreme material, cost, and energy challenges to desalination. Water disposal currently can cost ~ $47,000 - $400,000 per well for these oil/gas wells. In addition, concentration polarization, membrane fouling, and relatively low flux for processing large volume of produced waters continues to be a major concern for both commercial [1] and advanced membranes [9].

Table 1: Composition of Utica Shale flowback water (P_{osm} = 146 bar). Higher concentrations of sulphates, phosphates compared to ground water form tough scaling compounds, usually by combining with calcium and strontium posing extreme difficulty in membrane operations [10].

	Concentration (mg/l)		Concentration (mg/l)
TDS	184,000	Li^+	61.07 ± 0.07
Na^+	$49,250.19 \pm 125.97$	$Fe^{2+,3+}$	144.03 ± 1.51
Mg^{2+}	$1,831.76 \pm 9.55$	Mn^{2+}	8.6 ± 0.02
K^+	638.62 ± 3.74	Cl^-	$120,202.10 \pm 4922$
Ca^{2+}	$15,203.47 \pm 82.42$	Br^-	1380.20 ± 8.63
Si^{4+}	22.28 ± 0.53	F^-	2.25 ± 0.09
Sr^{2+}	$4,115.39 \pm 78.47$	SO_4^{2-}	113.25 ± 0.57
Ba^{2+}	$1,236.26 \pm 12.62$	PO_4^{3-}	20.904 ± 0.84

THEORETICAL BACKGROUND

Transport of ions, fluids, and small molecules across nanoscale conduits (with critical dimensions in the 1-100 nm range, defined as field of nanofluidics) in biological or many practically relevant miniature analytical systems is a growing technological impact area [11-13]. At these length scales, behavior of ions and fluids is dominated by fluid-surface interactions. Therefore, by passively and actively regulating the surface properties, local control of fluid and ions [14, 15] have been demonstrated. In this work, nanoscale fluid transport limited by interfacial phase change of water, governed by forward osmosis was used to desalt excessively saline solutions.

The equilibrium vapor pressure, P_{vap} of a salt solution with an osmotic pressure, Π, is given as

$$P_{vap} = P_{vap}^0 e^{\frac{-\Pi V_m}{R_g T}} \qquad (1)$$

where P_{vap}^0 is the equilibrium vapor pressure of pure water at Temperature T, V_m is molar volume of pure water at temperature T, and R_g is universal gas constant [9]. From

Eq. 1, it is evident that the vapor pressure of solution decreases exponentially with increase in osmotic pressure. Therefore, when two solutions of different osmotic pressure and hence different vapor pressure are trapped with their meniscus facing each other across a hydrophobic gap, the difference in vapor pressure drives a one-way transport of water as vapor from solution of lower concentration (feed) to higher concentrations (draw) (Fig. 1), forming the basis of vapor-transport based forward osmosis [9]. Since the vapor phase transport of water molecules begins with evaporation, all non-volatile species (e.g., salt) are rejected during this process, and thus a theoretical salt rejection of 100% is possible. Given that the mean free path for water vapor is 60 – 100 nm [9], the Knudsen number for an 80 nm deep channel was ~1, implying transitional flow.
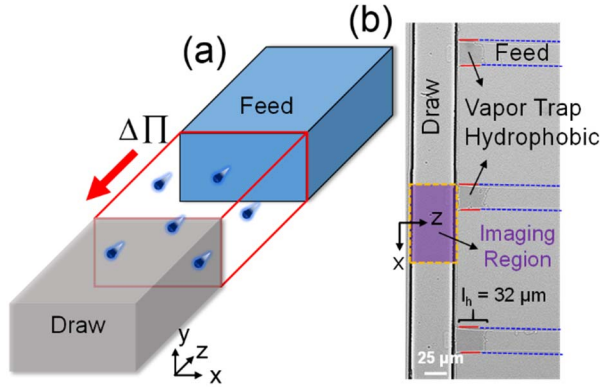

Figure 1: (a) Illustration of hydrophobic vapor trap sandwiched in-between opposing solution of different osmotic pressures. The hydrophobic region does not permit the liquid phase transport of water. (b) Microscope image showing a hydrophobic vapor trap of length l_h=32 μm separating the feed and draw solutions.

EXPERIMENTAL METHODS
Fabrication of prototype

To setup a proof-of-concept evaporation-condensation driven forward osmosis system, a set of three 80 nm deep (*H*) x 30 μm wide (*W*) and 2.5 mm long (*L*) nanochannels interconnecting two microchannels, 8 μm (*H*) x 50 μm (*W*) x 3 cm long (*L*) were patterned on borosilicate metal mask *via* UV lithography with several advances in fabrication reported previously [16]. Next, soda lime microscope slides with drilled access holes was bonded to the channel slide using known Ca-based bonding recipes [17] which has previously been shown to bond glass slides with μm deep channels. The bonding methodology as shown in Fig. 2a – c, was extended to bond 80 nm deep nanochannels in this work with greater than 90% usable device yields. Fig. 2d and Fig. 2e show the final bonded device and nanochannel-top cover interface respectively.

Surface Modification of Glass

The surface of the nanochannels were made hydrophobic by coating with a silane monolayer inside a nitrogen purged glove bag. Briefly, the prototype was flushed with isopropyl alcohol (IPA) and toluene before surface modification. Next, toluene was introduced in the feed microchannel, which also filled the entire nanochannel due to capillarity. Then, 1% v/v (heptadecafluoro-1,1,2,2-tetrahydrodecyl)trichlorosilane mixed with toluene in a second solution and introduced in the draw microchannel [18, 19]. The silane patterns a fluorine terminated hydrophobic monolayer inside the nanochannels, governed by diffusion [20]. The length of the hydrophobic region (l_h) was controlled by tuning the duration of silanization (Fig. 1b). After silanization, both feed and draw channels were emptied and triple rinsed with toluene, followed by IPA before introducing aqueous salts.
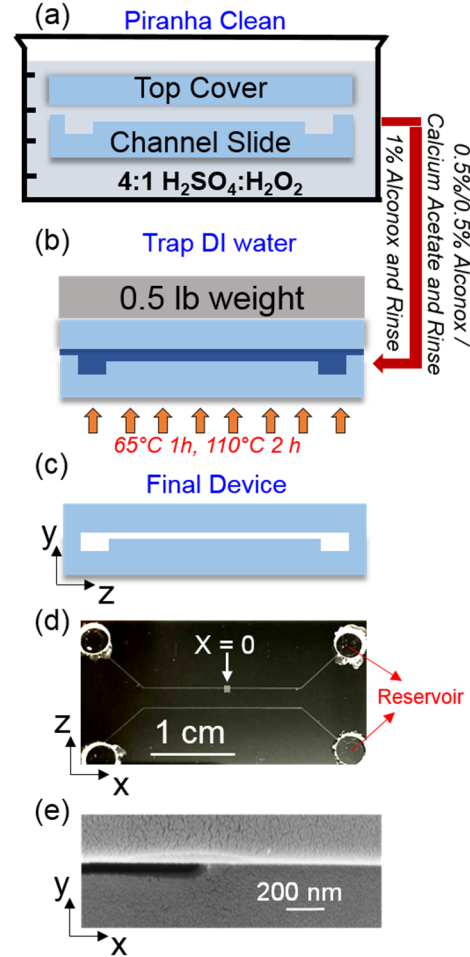

Figure 2: (a – c) Illustration of low temperature glass-glass bonding. (d) Photograph of final device showing microchannels. (e) Scanning electron microscope image showing part of an 80 nm deep nanochannel bonded without leaks with top cover.

RESULTS AND DISCUSSION
Prototype Characterization

Net flux due to the evaporation-condensation was estimated by filling the feed and draw microchannels with DI water and 1 M NaCl with 0.1 mM Rhodamine B (Rb), respectively. DI water fills the hydrophilic regions of the

nanochannel while the capillary pressure necessary to fill the hydrophobic barrier (advancing contact angle = 118.3° [18]) was in excess of 7.5 bar. Since no external pressure was applied, hydrophobic repulsion barricade liquid water from entering the functionalized region of nanochannels (Fig. 1), thereby trapping air. Intensity of Rb was monitored at the nanochannel - draw microchannel interface as shown in Fig. 1b for 1 hour for all experiments. This region is denoted by X = 0 (Fig. 2d).

Water evaporates from feed (higher vapor pressure) and condenses onto the draw microchannel (lower vapor pressure) (Fig. 1a). Condensation of pure water reduces the intensity of Rb dye by ~70% at imaging location, X = 0 (Fig. 1b) in draw channel over 1 h (Fig. 3b). To verify photo-bleaching was not the cause of reduction in Rb intensity, another experiment with $l_h = 0$ was conducted, where no reduction in Rb intensity was observed over a period of 1 h (Fig. 3a).
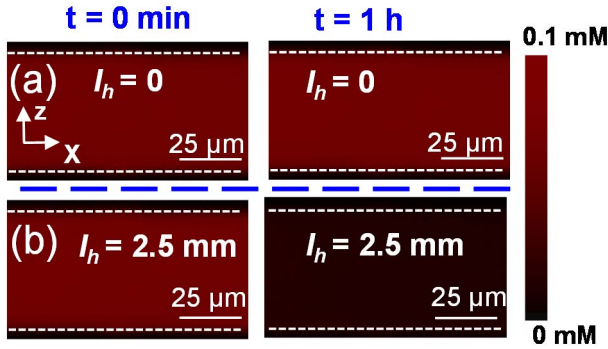

Figure 3: (a) No reduction in Rb intensity was observed when $l_h = 0$, while (b) 70% Reduction in Rb intensity in imaging region (x = 0) was observed for $l_h = 2.5$ mm in comparison to no change in intensity for $l_h = 0$.

Condensing water molecules move from the draw microchannel - vapor trap interface (X = 0) towards the reservoirs (X = 1.5 cm, Fig. 2d). To determine the water flux associated with the vapor transport, a numerical convection-diffusion model was implemented in COMSOL, which was solved transiently in the draw microchannel to fit the reduction in concentration of Rb, observed experimentally at X = 0 (Fig. 3). Intensity of Rb at t = 0 was assumed to be equal to initial Rb concentration of 0.1 mM.

The governing equation used for 1D (along *x-axis*) convection-diffusion model in the draw microchannel,

$$(\hat{x}\frac{\partial}{\partial x})\cdot\vec{u} = 0$$

$$\frac{\partial c}{\partial t} - (\hat{x}\frac{\partial}{\partial x})\cdot(D_i \frac{\partial}{\partial x}c) + \vec{u}\cdot(\hat{x}\frac{\partial c}{\partial x}) = 0 \qquad (2)$$

where $\hat{x}$ is unit vector along x, D_i is the diffusion coefficient of Rb (10^{-9} m^{2}s^{-1}), c, instantaneous concentration of Rb, and $\vec{u}$ instantaneous velocity of condensing water in draw microchannel. Though the flow is fully developed in the transverse directions (along *y, z-axis*), the convection-

diffusion equations were solved for the average velocity $\vec{u}$ along *x-axis*. This is because the transverse velocity distributions for a given average velocity can be readily known from the Poiseuille flow equations for a rectangular slit and which is well-established [21]. Secondly, solving for the average velocity and hence the average flux permits ready comparison with membrane permeation literature [1]. It is important to note that the diffusive flux acts against the direction of convective flux and therefore regions close to the end of draw microchannel (X = 1.5 cm) did not show any drop in intensity of Rb over 1 h. Therefore, Rb concentration at the outlet was fixed to 0.1 mM in the numerical models. The boundary conditions were:

$$c\,[0,x] = 0.1\,mM$$
$$c\,[t,1.5\,cm] = 0.1\,mM \qquad (3)$$

Fig. 4 shows the spatial distribution of Rb obtained from the model solved for 1 h. The concentration of Rb from the model was matched with the experimentally obtained concentration of Rb at X = 0 over 1 h. The velocity was averaged over 1 h to estimate the average flux. By tuning l_h, = 32 µm, (Fig. 1b), a maximum flux of 47.3 Lm^{-2}h^{-1} was estimated for the present study in comparison to 10 Lm^{-2}h^{-1} for state-of-art FO membranes.
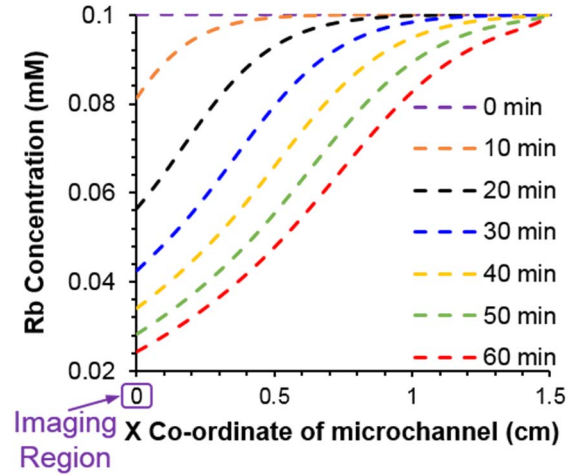

Figure 4: Rb concentration distribution across draw channel was estimated by solving transient numerical convection-diffusion equation in COMSOL. Numerically estimated Rb concentration with time matched the experimentally observed Rb concentration at imaging region, X=0.

Additionally, the hydrophobic barrier prevented back flow of draw water to feed water when tested over 40 cycles reducing uncertainty in flux estimation.

Testing with Utica Shale Flowback Water

Next, direct Utica shale flowback water (184,000 ppm TDS; Table 1) was used as draw with minimal pre-treatment to remove large (>20 µm) particulates, in yet another prototype with l_h tuned to 112 µm. Dilution in the draw

microchannel was visualized by tagging free Na$^+$ in flowback solution with 0.1 mM CoroNa Green *(Cg, $\lambda_{ex}/\lambda_{em}$ = 492/516 nm)* with feed, containing 0.1 mM Rb. In an hour, 92% reduction in intensity for CoroNa Green translated to an average water flux of 46.2 Lm^{-2}h^{-1} leading to desalting of the shale flowback water from 184,000 ppm to 14,720 ppm. Over the same time, ~99.9% Rb rejection from the feed was observed for salt rejection quantification. On-going research targets significant scale-up using wafer-scale fabrication of nanochannels to run experiments with larger volumes. Therefore, nanoscale vapor-traps permit water transport *via* evaporation and condensation from feed to draw while rejecting non-volatile ions from the feed. More importantly, the functionality of the prototype was sustained even in highly salty water.

REFERENCES

[1] E. R. Cornelissen, *et al.*, "Membrane fouling and process performance of forward osmosis membranes on activated sludge," *Journal of Membrane Science,* vol. 319, p. 158-168, 2008.

[2] S. Chu and A. Majumdar, "Opportunities and challenges for a sustainable energy future," *Nature,* vol. 488, p. 294-303, 2012.

[3] http://www.eia.gov/electricity/monthly

[4] P. Jaramillo, *et al.*, "Comparative Life-Cycle Air Emissions of Coal, Domestic Natural Gas, LNG, and SNG for Electricity Generation," *Environmental Science & Technology,* vol. 41, p. 6290-6296, 2007.

[5] http://geosurvey.ohiodnr.gov

[6] N. R. Warner, *et al.*, "Impacts of Shale Gas Wastewater Disposal on Water Quality in Western Pennsylvania," *Environmental Science & Technology,* vol. 47, p. 11849-11857, 2013.

[7] https://www.epa.gov/uic/class-ii-oil-and-gas-related-injection-wells

[8] F. R. Walsh and M. D. Zoback, "Oklahoma's recent earthquakes and saltwater disposal," *Science Advances,* vol. 1, 2015.

[9] J. Lee, T. Laoui, and R. Karnik, "Nanofluidic transport governed by the liquid/vapour interface," *Nature Nanotechnology,* vol. 9, p. 317-323, 2014.

[10] S. P. Chesters, "Innovations in the inhibition and cleaning of reverse osmosis membrane scaling and fouling," *Desalination,* vol. 238, p. 22-29, 2009.

[11] L. Bocquet and E. Charlaix, "Nanofluidics, from bulk to interfaces," *Chemical Society Reviews,* vol. 39, p. 1073-1095, 2010.

[12] S. Prakash and J. Yeom, *Nanofluidics and Microfluidics: Systems and Applications*. Norwich, NY: William Andrew, 2014.

[13] S. Prakash and A. T. Conlisk, "Field effect nanofluidics," *Lab on a Chip,* vol. 16, p. 3855-3865, 2016.

[14] M. Fuest, *et al.*, "A Three-State Nanofluidic Field Effect Switch," *Nano Letters,* vol. 15, p. 2365–2371, 2015.

[15] M. Fuest, *et al.*, "Active surface potential control for artificial ion pumps," in *Solid State Sensors and Actuator Workshop*, Hilton Head Island, SC, 2014.

[16] M. Pinti, *et al.*, "Fabrication of Centimeter Long, Ultra-Low Aspect Ratio Nanochannel Networks in Borosilicate Glass Substrates," *Journal of Nanotechnology in Engineering and Medicine,* vol. 4, p. 020905, 2013.

[17] P. B. Allen and D. T. Chiu, "Calcium-Assisted Glass-to-Glass Bonding for Fabrication of Glass Microfluidic Devices," *Analytical Chemistry,* vol. 80, p. 7153-7157, 2008.

[18] K. K. Rangharajan, *et al.*, "Effect of surface modification on interfacial nanobubble morphology and contact line tension," *Soft Matter,* vol. 11, p. 5214-5223, 2015.

[19] S. Prakash, *et al.*, ""Click" Modification of Silica Surfaces and Glass Microfluidic Channels," *Analytical Chemistry,* vol. 79, p. 1661-1667, 2007.

[20] R. Karnik, *et al.*, "Diffusion-Limited Patterning of Molecules in Nanofluidic Channels," *Nano Letters,* vol. 6, p. 1735-1740, 2006.

[21] N. A. Mortensen, *et al.*, "Reexamination of Hagen-Poiseuille flow: Shape dependence of the hydraulic resistance in microchannels," *Physical Review E,* Vol. 71, p. 057301, 2005.